JAMES | Journal of Advances in Modeling Earth Systems®

RESEARCH ARTICLE
10.1029/2022MS003045

Special Section:
Using radiative-convective equilibrium to understand convective organization, clouds, and tropical climate

Congestus Mode Invigoration by Convective Aggregation in Simulations of Radiative-Convective Equilibrium

Adam B. Sokol[1] **and Dennis L. Hartmann**[1]

[1]Department of Atmospheric Sciences, University of Washington, Seattle, WA, USA

Key Points:

- Representation of the congestus mode in RCE varies greatly across models
- The congestus mode is invigorated by large-scale convective aggregation
- Tropospheric stability increases with aggregation due to congestus invigoration and reduced entrainment cooling

Supporting Information:

Supporting Information may be found in the online version of this article.

Correspondence to:

A. B. Sokol,
abs66@uw.edu

Citation:

Sokol, A. B., & Hartmann, D. L. (2022). Congestus mode invigoration by convective aggregation in simulations of radiative-convective equilibrium. *Journal of Advances in Modeling Earth Systems*, *14*, e2022MS003045. https://doi.org/10.1029/2022MS003045

Received 13 FEB 2022
Accepted 8 JUN 2022

Abstract This study examines how the congestus mode of tropical convection is expressed in numerical simulations of radiative-convective equilibrium (RCE). We draw insights from the ensemble of cloud-resolving models participating in the RCE Model Intercomparison Project (RCEMIP) and from a new ensemble of two-dimensional RCE simulations. About half of the RCEMIP models produce a congestus circulation that is distinct from the deep and shallow modes. In both ensembles, the congestus circulation strengthens with large-scale convective aggregation, and in the 2D ensemble this comes at the expense of the shallow circulation centered at the top of the boundary layer. Congestus invigoration occurs because aggregation dries out the upper troposphere, which allows moist congestus outflow to undergo strong radiative cooling. The cooling generates divergence that promotes continued congestus overturning (a positive feedback). This mechanism is fundamentally similar to the driving of shallow circulations by radiative cooling at the top of the surface boundary layer. Aggregation and congestus invigoration are also associated with enhanced static stability throughout the troposphere, but a modeling experiment shows that enhanced stability is not necessary for congestus invigoration; rather, invigoration itself contributes to the stability increase via its impact on the vertical profile of radiative cooling. Changes in entrainment cooling are also found to play an important role in stability enhancement, as has been suggested previously. When present, congestus circulations have a large impact on the mean RCE atmospheric state; for this reason, their inconsistent representation in models and their impact on the real tropical atmosphere warrant further scrutiny.

Plain Language Summary Atmospheric convection over tropical oceans has three distinct types that differ in their vertical reach: a deep mode typically associated with towering cumulonimbus clouds, a shallow mode restricted to the lowest ∼2 km of the atmosphere, and a congestus mode that falls somewhere in between. This study focuses on the congestus mode, which has received comparatively little attention in the past. We investigate the sources of congestus mode variability in simple simulations of the tropical atmosphere. The congestus mode is expressed very strongly in some models but is absent in others. We find that it is stronger when convection is clumped into a limited portion of the model domain rather than dispersed. When present, the congestus mode has a big impact on the distribution of temperature and moisture throughout the atmosphere. These results are important because they help us better understand the nature of the congestus mode and the climates produced by commonly used atmospheric models.

1. Introduction

Convection in the tropical atmosphere is known to be trimodal (Johnson et al., 1999). The first and dominant mode is deep convection, marked by towering cumulonimbus clouds extending from the boundary layer to the tropopause. Deep convection is typically front and center in conceptual models of the tropical circulation because of its close relationship to the Hadley and Walker circulations, which play an important role in global climate. The second mode is shallow convection, which produces shallow cumulus clouds (also called trade wind cumulus) at the top of the boundary layer. The final mode, the congestus mode, describes convection that reaches the mid-troposphere. Congestus cloud tops are typically found in the vicinity of the freezing level, distinctly between shallow and deep cumulus. This third mode is the primary focus of this paper.

In previous work, the term *shallow* has often been used to refer to any convective feature that is distinct from the deep mode. But such features could be either shallow or congestus in nature; to avoid this ambiguity, we refer to features as *shallow* if they are restricted to pressures greater than 750 hPa and *congestus* if their upper extent lies between 400 and 750 hPa.

The three modes of tropical convection were first recognized by Johnson et al., 1999 in the observed distribution of clouds over tropical oceans. However, overturning circulations observed in the tropics or derived from global wind reanalyzes have generally been only bimodal, with a deep mode and a second mode that is either shallow, congestus, or something in between (Schulz & Stevens, 2018; Trenberth et al., 2000; Y.-C. Chen & Yu, 2021; Zhang et al., 2004, 2008). There are several possible explanations for this discrepancy. It could be the case that the three modes are not expressed simultaneously, or that the shallow and congestus modes fuse together when averaged over large regions or periods of time. It could also be the case that the relatively fine structures of the shallow mode are not well resolved in reanalyzes. Or, perhaps the shallow and congestus modes of convection simply do not translate into distinct modes of the tropical overturning circulation due to interference from other dynamical factors.

The situation is somewhat different in model simulations of radiative-convective equilibrium (RCE), in which each mode of convection is associated with a closed overturning circulation. This is because traditional "RCE-in-a-box" simulations, unlike the real tropics, have no mean large-scale vertical motion, so all convective detrainment must be compensated for by subsidence at the same vertical level. Many model simulations successfully capture the trimodal character of convection (Beydoun & Hoose, 2019; Bretherton et al., 2006; C. J. Muller & Held, 2012; Holloway & Woolnough, 2016; Posselt et al., 2008; Y.-T. Chen & Wu, 2019), but others produce just two modes (Arnold & Putman, 2018; Grabowski et al., 2000; Nolan et al., 2007). The congestus mode is especially fickle but has received little attention compared to the deep and shallow modes. Our primary goal here is to better understand the variability and sensitivities of the congestus mode in simulated RCE.

Previous work has provided valuable insights into the nature of congestus overturning. Yano et al. (2002) argued that cloud-resolving models (CRMs) develop congestus-like circulations (what they refer to as "shallow double-cell" circulations) because the deep circulation is linearly unstable when the model domain is a few thousand kilometers in length. The deviation of model temperature profiles from the real atmosphere has also been implicated (Grabowski et al., 2000). Others have described congestus convection as a precursor to deep convection that imports moist static energy until the latent heating is strong enough to support deep updrafts (Masunaga & L'Ecuyer, 2014; Wu, 2003; Y.-C. Chen & Yu, 2021). Additionally, congestus clouds have long been associated with mid-tropospheric stable layers, which are thought to inhibit the vertical development of convection by reducing updraft buoyancy and promoting midlevel detrainment. These stable layers have been attributed to various causes, including: Latent cooling associated with the melting of frozen precipitation from stratiform clouds (B. E. Mapes & Houze, 1995; Johnson et al., 1996; Yasunaga et al., 2006); evaporative cooling of detrained liquid condensate and subsequent radiative cooling (Nuijens & Emanuel, 2018; Posselt et al., 2008); and the radiative (B. E. Mapes & Zuidema, 1996) and microphysical (Zuidema et al., 2006) responses to dry air intrusions. This previous work suggests that careful consideration of moisture, radiative transfer, and static stability is necessary in order to fully understand how the congestus mode is expressed in cloud-resolving RCE.

The apparent linkages to moisture and static stability also beg the question of how the congestus mode is affected by the large-scale self-aggregation of convection (*aggregation* for brevity). Aggregation describes the process by which convection spontaneously organizes into distinct regions characterized either by mean ascent (the *moist* or *convecting* regions) or by radiatively driven subsidence (the *dry* or *nonconvecting* regions). The convecting and nonconvecting regions correspond to the rising and subsiding branches, respectively, of the convectively coupled circulation modes. Aggregation affects the mean RCE climate in several important ways, two of which will be especially relevant throughout this paper. First, the troposphere becomes warmer and more stable (Bretherton et al., 2005; Held et al., 1993; Wing & Cronin, 2016). Because stable layers are thought to promote congestus-level detrainment, we may a priori expect the congestus circulation to strengthen in response to aggregation. Second, the troposphere becomes drier on average as the dry, nonconvecting regions grow to occupy a large fraction of the horizontal area (Bretherton et al., 2005). Dryness aloft allows for strong radiative cooling at the top of the moist boundary layer in nonconvecting regions, which is thought to play an important role in driving shallow circulations (Bretherton et al., 2005; Naumann et al., 2017, 2019; Nigam, 1997; Nishant et al., 2016). These shallow circulations have been shown to support aggregation by transporting moist static energy up-gradient from nonconvecting to convecting regions (Bretherton et al., 2005; C. J. Muller & Held, 2012; C. Muller & Bony, 2015; Schulz & Stevens, 2018). Despite an extensive study of convective aggregation, its impact on congestus circulations has, to our knowledge, not been investigated.

This paper explores three different aspects of the congestus mode in cloud-resolving RCE. First, we seek to understand its intermodel variability. To do so, we examine the circulation structures produced by the ensemble of CRMs participating in the Radiative-Convective Equilibrium Model Intercomparison Project (RCEMIP; Wing et al., 2018). Beyond contributing to the ongoing exposition of RCEMIP results, which is valuable in its own right, this analysis will illustrate that different models produce very different RCE circulations even when the experimental configurations are identical. It will also show that stronger congestus circulations are associated with higher degrees of convective aggregation and greater tropospheric stability.

Second, we ask why the congestus circulation is invigorated by convective aggregation. This question is difficult to answer using the RCEMIP ensemble, since the RCEMIP models differ in countless ways. We overcome this difficulty by performing a new set of idealized, two-dimensional RCE simulations that use a single model but span a wide range of aggregation states, which offers a more compelling account of the relationship between aggregation, congestus strength, and static stability. In this new ensemble, aggregation invigorates the congestus circulation at the expense of the shallow circulation. We will show that the congestus circulation is subject to a positive feedback involving vertical gradients of moisture and radiative cooling. An additional simulation with prescribed radiative cooling will show that this feedback is central to congestus invigoration, whereas greater tropospheric stability is not necessary.

Lastly, we investigate why the troposphere is more stable when convection is aggregated. This will show that congestus invigoration is a cause, rather than a consequence, of enhanced stability. Previously identified sources of enhanced stability are also found to play an important role.

In Section 2, we describe the RCEMIP model output, explain the transformation to "moisture space" used to characterize atmospheric circulations, and discuss the RCEMIP results. In Section 3, we introduce the new, 2D simulations and investigate the causes of congestus invigoration. Section 4 focuses on static stability, its dependence on aggregation, and its relationship to the congestus mode. In Section 5, we summarize and discuss our results.

2. Circulation Variability in the RCEMIP CRM Ensemble

2.1. Simulations and Output

The RCEMIP simulation protocol is described in Wing et al. (2018). We use output from the "RCE_large300" CRM runs obtained from the public RCEMIP repository hosted by the German Climate Computing Center. We refer to the different models using the same naming conventions as in Wing et al. (2020). There are 12 CRMs for which full RCE_large300 output is available at the time of writing; all are included in our analysis with the exception of the UKMO-RA1-T-nocloud simulation, which differs from the UKMO-RA1-T run (which we include) only wherinsub-grid cloud scheme is disabled.

The RCE_large300 simulations use a domain size of ∼6,000 km × ∼400 km, a horizontal grid spacing of 3 km, and a uniform sea surface temperature (SST) of 300 K. There is no rotation. Each model run was integrated for at least 100 days. Our analysis uses the last 25 days of each simulation, for which instantaneous 3D output is available at six-hour intervals. An exception to these specifications is the DAM model, which has 2.5-km horizontal grid spacing and 3D output available at 24-hr intervals. The RCEMIP CRMs use a variety of vertical coordinates. To facilitate comparison across models, we convert all output to pressure coordinates by taking the time- and domain-averaged pressure at each vertical level.

In addition to the 11 RCEMIP simulations, we conduct a new, RCEMIP-style run using the System for Atmospheric Modeling (SAM; Khairoutdinov & Randall, 2003) with the Predicted Particle Properties (P3) microphysics scheme (Morrison & Milbrandt, 2015) and RRTM radiation (Iacono et al., 2000; Mlawer et al., 1997). We will refer to this run as SAM-P3 to distinguish it from the RCEMIP SAM-CRM run, which uses a different microphysics scheme. The SAM-P3 run uses a 6,144 × 384-km^2 domain. All other specifications (horizontal resolution, vertical grid, insolation, and trace gases, etc.) follow the RCEMIP protocol for RCE_large300 simulations.

2.2. Transformation to Moisture Space

We will examine atmospheric circulations in "moisture space", as has been done in the past (e.g., Bretherton et al., 2005; Beydoun & Hoose, 2019; Holloway & Woolnough, 2016; Schulz & Stevens, 2018). In this approach,

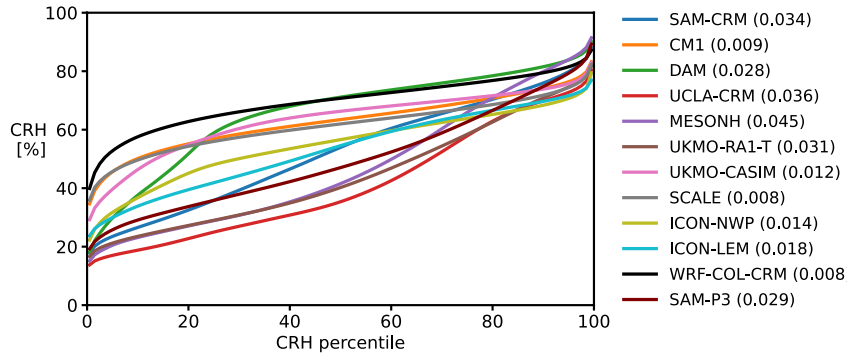

Figure 1. Column relative humidity (CRH) percentiles for the RCEMIP cloud-resolving models (RCE_large300 simulations). The CRH variance σ^2_{CRH} for each model is given in parentheses.

vertical columns of the atmosphere are rearranged and binned according to some measure of column-integrated moisture; here, we use the column relative humidity (CRH) percentile. Because horizontal temperature gradients are weak in the tropics (Sobel et al., 2001), CRH corresponds closely to the column-integrated moist static energy. We use all of the model output from the 25-day compositing period to compute the mean atmospheric state as a function of CRH percentile. The result is a transformation of the modeled atmosphere from four dimensions (x, y, p, and t) to two (CRH percentile, p). The circulations that emerge from this transformation reflect the exchange of mass between moist regions typically associated with convection and dry regions associated with subsidence.

For each simulation, we begin by computing CRH for each atmospheric column at every time step in the 25-day compositing period for which 3D output is available. CRH is computed from the 2D output as the ratio of the column-integrated water vapor to the saturation column-integrated water vapor. The calculation of saturation vapor pressure is not specified in the RCEMIP protocol and therefore varies from model to model. CRH percentiles are then assigned to each grid cell at each time step; the percentiles are computed relative to the entire set of CRH values for the 25-day compositing period, as opposed to the values from each individual time step. The grid cells are then sorted by CRH percentile into 100 equally sized bins, with each bin thus representing 1% of the domain area over time.

Figure 1 shows the CRH percentiles for each of the RCEMIP models. Differences in the curves reflect intermodel differences in how moisture is distributed across the domain, which are closely related to differences in the degree of convective aggregation. In this paper, we quantify the degree of aggregation using the spatial and temporal variance of CRH $\left(\sigma^2_{\mathrm{CRH}}\right)$, which has been used by others in the past (Wing et al., 2020). We prefer this metric because it is simple and physically intuitive within the moisture space context. Figure 1 shows that the models are tightly clustered when it comes to the CRH in the moistest part of the domain. The intermodel spread is much larger in the driest regions, suggesting that σ^2_{CRH} is determined primarily by how dry the dry regions become.

Following Schulz and Stevens (2018), we compute the mass stream function Ψ (kg m^{-2} s^{-1}) in pressure coordinates as

$$\Psi_i(p) = \Psi_{i-1}(p) + \frac{\alpha}{g}\omega_i(p) \tag{1}$$

where i is the CRH percentile bin rank (1–100) and $\Psi_0(p) = 0$. ω is the bin-averaged vertical velocity in pressure coordinates, g is the acceleration due to gravity, and $\alpha = 0.01$ is the fraction of total grid boxes contained in the i-th bin. The algebraic sign of Ψ is such that flow is counterclockwise around Ψ maxima and clockwise around Ψ minima in all subsequent figures.

From Ψ, we can compute the horizontal velocity in moisture space, v, as

$$v_i(p) = -g\frac{\partial \Psi_i(p)}{\partial p}. \tag{2}$$

v represents the horizontal exchange of mass between CRH percentile bins. It has unconventional units of time^{-1} because, in moisture space, "distance" is measured as a dimensionless fraction of the domain area. We have chosen these particular formulations of Ψ and v because they are independent of domain size, which varies slightly across the RCEMIP ensemble for computational reasons. They are also easily applicable in both two and three dimensions, allowing us to use the same formulations in our analysis of the 2D ensemble in Section 3.

In moisture space, we quantify the strength of the congestus circulation as v_{cong}, equal to the 400–750-hPa mass average of the negative values of v at the 50th CRH percentile. The 400–750-hPa range was chosen because it excludes outflow associated with the deep and shallow circulations but captures the range of congestus detrainment heights produced by the different simulations. If v is positive throughout this entire range, as it is in two of the RCEMIP models (SCALE and WRF-COL-CRM), v_{cong} is set to zero. More negative values of v_{cong} indicate stronger congestus-level flow from high to low CRH and thus a stronger congestus circulation.

2.3. Circulation

Stream functions (Ψ) for the RCEMIP models are shown in Figure 2a. While there is clearly a great diversity among the models, there are some common features to note. All models produce a dominant deep circulation that extends from the lower troposphere to ∼200 hPa. The rising branches of the deep cells are confined to the top few CRH percentiles, meaning that the upward convective mass flux is concentrated within a small horizontal area. A majority of the models have negative Ψ near the surface in the top few CRH percentiles, which is the signature of below-cloud downdrafts driven by the evaporative cooling of rain (i.e., cold pools).

The deep circulation in ICON-NWP is unique in several ways. First, the rising branch extends to much lower CRH percentiles than in the other runs. This does not mean that updrafts occupy a larger fraction of the domain (they do not), but that ω is not tightly linked to CRH in ICON-NWP. Second, the deep overturning circulation is weak compared to those in the other models. This is consistent with the previous finding that the integrated, atmospheric radiative cooling rate is smaller in ICON-NWP than in any other RCEMIP model, including the general circulation models (see R_{Net} in Table A2 in Wing el al., 2020). The weak atmospheric cooling is partially due to especially high cloud fraction in the upper troposphere (Figure 2b). The ubiquitous high clouds are also responsible for the distinct circulation cell between 150 and 300 hPa that flows in the opposite direction as the deep cell, with ascent in dry regions and subsidence in moist regions. This circulation is driven by cloud radiative effects, which heat the upper troposphere at low CRH and cool it at high CRH (Figure 2c).

Shallow circulations centered near the top of the boundary layer are present in a majority of the models. As one would expect from previous work, the models with strong shallow circulations are generally those with strong radiative cooling at the top of the dry-region boundary layer (Figure 2c). This cooling is remarkably strong in UCLA-CRM due to the combination of high humidity and cloud fraction within the boundary layer and low humidity immediately above.

The most notable difference between the model circulations is the representation of the congestus mode. In the moisture-space framework, the clearest marker of the congestus circulation is its upper branch, which manifests as a layer of moist-to-dry outflow (negative v) in the mid-troposphere. UCLA-CRM and SAM-P3 produce distinct congestus cells with outflow between 400 and 600 hPa (Figure 2a). MESONH also has a trimodal circulation with lower outflow layers at 400–500 and 650–800 hPa. UKMO-CASIM and DAM both have weak congestus outflow layers, although in DAM the flow is restricted to low CRH percentiles, which suggests that it may not originate from surface-based convection. Interestingly, UKMO-RA1-T produces a circulation with four distinct cells, the middle two of which have outflow in the congestus range. The remaining models produce bimodal circulations without a congestus cell.

When present, the congestus circulation has a large impact on relative humidity (RH; Figure 2b) and radiative cooling (Figure 2c). Congestus outflow layers are associated with plumes of moisture extending from the convective regions into the nonconvective regions, which tend to be drier in the runs with strong congestus cells. As the moist outflow travels away from its convective source, the atmosphere above it becomes increasing dry, and a strong vertical gradient in RH develops at the top of the outflow layer. The sharp drop-off in RH with height allows for strong radiative cooling, which causes the layer to gradually subside as it moves further from convection. This structure is most evident in UCLA-CRM, UKMO-RA1-T, and SAM-P3.

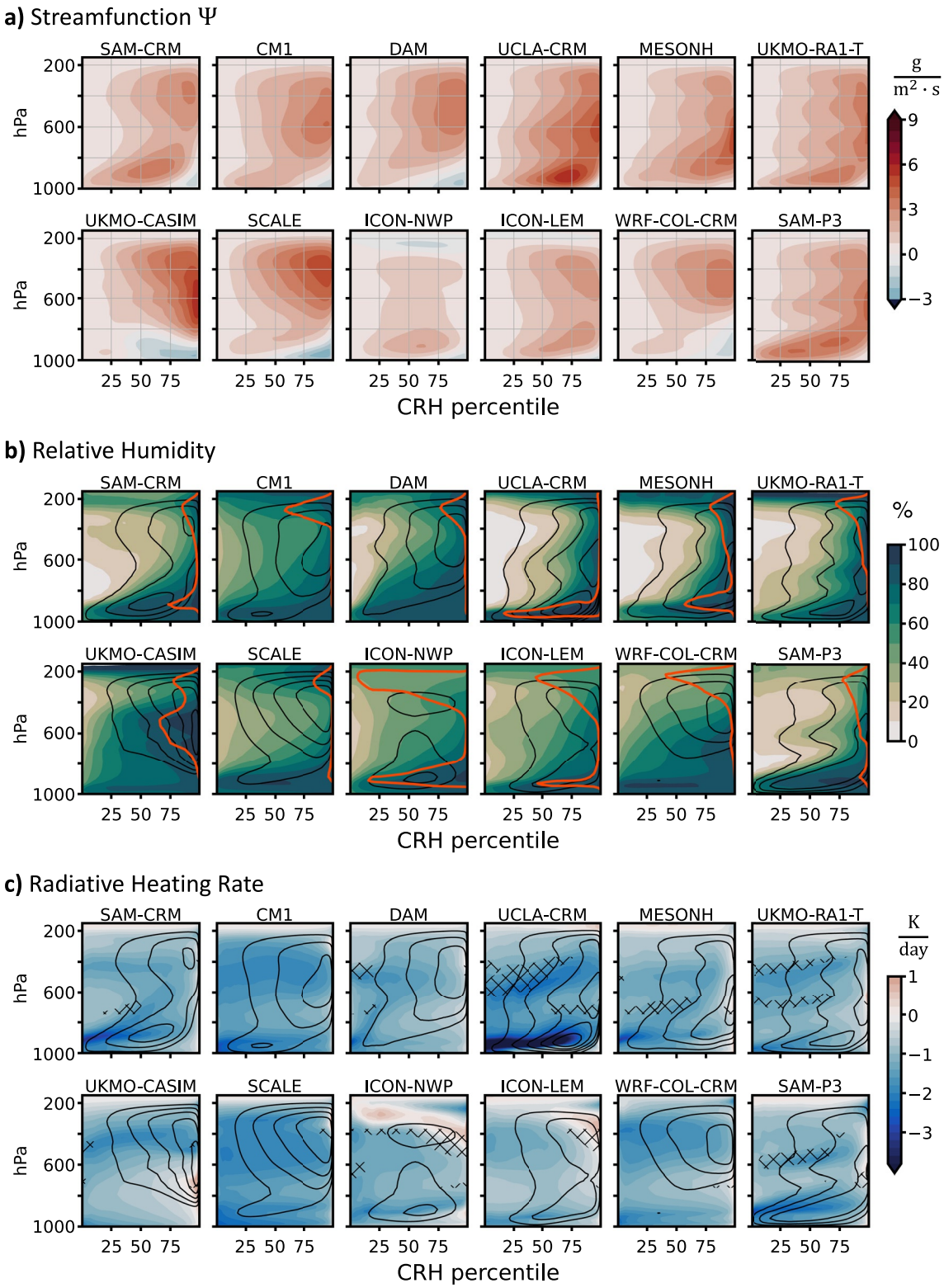

Figure 2. (a) Stream function Ψ, (b) relative humidity, and (c) radiative heating rate in moisture space for the RCEMIP CRMs. The black contours in (b) and (c) show Ψ and have a spacing of 1 g m^{-2} s^{-1} (the outermost contour is 1 g m^{-2} s^{-1}). Flow is counterclockwise around Ψ maxima. The orange contour in (b) indicates a cloud fraction of 0.1 using a cloud condensate threshold of 10^{-5} kg kg^{-1}. The hatching in (c) shows where the radiatively driven divergence D_{rad} exceeds 0.05 day^{-1}; hatching is only shown between 350 and 750 hPa. Note: Ψ closes (goes nearly to zero) at the highest CRH percentile.

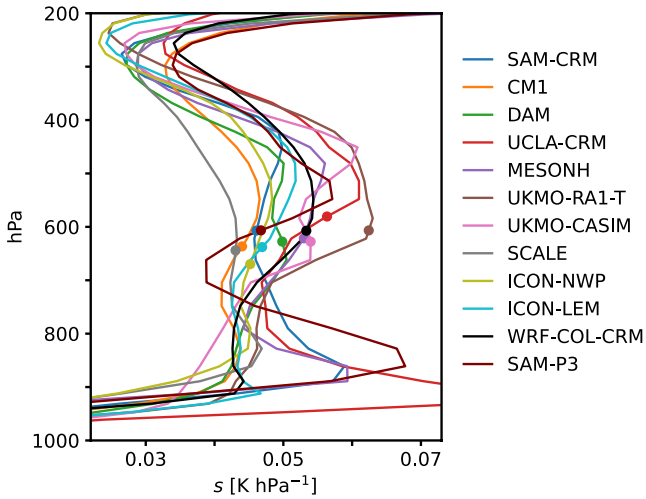

Figure 3. Domain-averaged static stability s for each RCEMIP CRM. Dots indicate the freezing level for each run.

The sharp vertical gradients in RH and radiative cooling are similar in many respects to those thought to induce shallow circulations at the top of the boundary layer (Bretherton et al., 2005; Naumann et al., 2017). It is easy to envision an analogous mechanism acting as a positive feedback on congestus detrainment. Because horizontal temperature gradients in tropical RCE are weak, the dominant thermodynamic balance in the free troposphere in nonconvective regions is that between radiative cooling and subsidence warming. The rate of subsidence needed to exactly balance radiative cooling is $\omega_{\text{rad}} = Q_{\text{rad}}/s$, where Q_{rad} is the radiative cooling rate and s the static stability. In nonconvective regions, where radiative cooling is the principal diabatic process, ω_{rad} is a good approximation of mean ω. Vertical gradients in ω_{rad} produce radiatively driven divergence

$$D_{\text{rad}} = \frac{\partial}{\partial p}\omega_{\text{rad}}. \tag{3}$$

To satisfy mass continuity, radiatively driven divergence in nonconvective regions must be filled by horizontal outflow from convective regions at the same vertical level. These outflow plumes undergo strong cooling, which generates radiatively driven divergence and, in turn, leads to more congestus outflow. We will refer to this as the *radiative-divergence feedback*.

The hatching in Figure 2c indicates D_{rad} in excess of 0.05 day^{-1}. While every model produces widespread divergence above 300 hPa associated with the deep mode, hatching is only shown between 350 and 750 hPa for clarity. About half of the models have notable divergence within this pressure range. In the two ICON models, the divergence is associated with cloud radiative heating. In the others, it is coincident with the top of the congestus outflow layer, where the radiative cooling rate rapidly decreases with height. This shows that the patterns of radiative cooling produced by congestus detrainment are qualitatively consistent with the radiative-divergence feedback mechanism.

2.4. Static Stability and Aggregation

As previously discussed, static stability may also play an important role in congestus dynamics. Figure 3 shows the mean static stability for each RCEMIP model, which in pressure coordinates is given by

$$s = -\frac{T}{\theta}\frac{\partial \theta}{\partial p} \tag{4}$$

All of the models produce relative maxima somewhere between 400 and 650 hPa. In a few of the models, the maxima are located very close to the freezing level (indicated by the colored dots), suggesting that they are directly related to microphysical phase transitions. In the other models, the maxima are generally located above the freezing level. Apart from large differences in stability at the top of the boundary layer, the intermodel spread is greatest near the midlevel maxima. This is likely due to differences in entrainment and microphysical processes between the models, which may in turn be related to the degree of convective aggregation. Vertical gradients in Q_{rad} may also contribute to the spread in stability, as will be discussed in Section 4. There is much better model agreement in the upper troposphere (250–400 hPa), where water vapor is scarce and the lapse rate is constrained to be close to the dry adiabatic limit.

We turn now to the question of how stability, aggregation, and congestus strength covary across the RCEMIP ensemble. Correlation coefficients for these three factors, along with the midlevel D_{rad} in nonconvective regions, are provided in Table 1.

As expected from previous work, aggregation is generally associated with greater midlevel stability. But σ^2_{CRH} explains only about a quarter of the vari-

Table 1
Correlation Coefficients for Measures of Convective Aggregation (σ^2_{CRH}), Congestus Strength (v_{cong}), Midlevel Stability (s), and Radiatively Driven Divergence (D_{rad}) Across the RCEMIP Ensemble of CRMs

	σ^2_{CRH}	v_{cong} [a]	s [b]	D_{rad} [c]
σ^2_{CRH}	1.00	−0.82	0.52	0.84
v_{cong} [a]	−0.82	1.00	−0.63	−0.81
s [b]	0.52	−0.63	1.00	0.66
D_{rad} [c]	0.84	−0.81	0.66	1.00

[a]v_{cong} decreases with increasing congestus strength. [b]400–600-hPa mean. [c]400–750-hPa and 1–50th-CRH percentile mean.

ance in stability ($r^2 = 0.52^2 = 0.27$), suggesting that other factors are just as important. This is not particularly surprising; the many differences in model physics across the RCEMIP ensemble will impact the stability in a variety of ways, which limits the explanatory power of any single quantity such as σ^2_{CRH}.

Congestus strength is generally associated with greater aggregation and midlevel stability. Our a priori reasoning was that aggregation could invigorate the congestus circulation precisely through its impacts on stability. Therefore, it is somewhat surprising that v_{cong} is more tightly linked to σ^2_{CRH} than to s (Table 1). This alone does not dismiss the importance of stability, but it does invite us to consider alternative explanations for why the congestus circulation strengthens with aggregation.

One such explanation may be the radiative-divergence feedback identified in the previous section. Congestus-level D_{rad} and v_{cong} are strongly correlated across the RCEMIP ensemble, which is to be expected from basic mass continuity constraints. Less obvious is the strong relationship between D_{rad} and σ^2_{CRH}, which we may expect now given both variables' relationships with v_{cong} but which we did not expect a priori. These results raise the possibility that congestus invigoration is caused not by increasing stability but rather by the activation of the radiative-divergence feedback. If this is the case, the relationship between stability and v_{cong} may simply reflect underlying changes in aggregation rather than a causal link; this relationship will be revisited in Section 4.

We have now identified two possible mechanisms of congestus invigoration: the stability mechanism—In which increasing stability with aggregation reduces updraft buoyancy and promotes congestus-level detrainment—And the radiative-divergence mechanism, in which aggregation activates the radiative-divergence feedback. This leaves us with two important questions: How, physically, does aggregation affect the radiative-divergence feedback? And what is the relative importance of the two mechanisms? It is difficult to pursue these questions further using the RCEMIP output, since the output variables are limited and the various relationships in question are complicated by myriad differences in model physics. For these reasons, we turn now to the new ensemble of 2D simulations.

2.5. Summary

- Some RCEMIP CRMs simulate trimodal convection, while others produce bimodal convection. One model produces a circulation with four modes.
- Through its impacts on moisture and radiative cooling, the congestus circulation is subject to a positive feedback (the radiative-divergence feedback).
- Aggregation is associated with congestus invigoration and with midlevel increases in stability and radiatively driven divergence.

3. Congestus Invigoration in Two-Dimensional RCE

3.1. Model Simulations

Our goal with the new 2D simulations is to examine the relationship between aggregation, stability, and congestus strength in the absence of other changes in model physics. To do this, we will use a single model (SAM) and microphysics scheme (P3) to generate a range of equilibria with varying degrees of aggregation and tropospheric stability. The two-dimensional domain makes the runs computationally efficient and allows us to simulate a large number of aggregation states.

The control run is a normal RCE run with uniform 300-K SSTs. In the other runs, we apply small adjustments to the model physics or configuration that are thought to impact aggregation and stability in some way. The adjustments are listed in Table 2. With the exception of the control run, each simulation uses a unique combination of up to three adjustments. There are 20 runs in total.

This experimental approach allows us to interpret ensemble trends with confidence. On their own, each model adjustment may introduce confounding factors that would make it difficult to interpret changes in congestus strength. But any physical relationships gathered from the full ensemble of simulations are unlikely to be spurious, since the adjustments target completely different parts of the model setup and code. The full ensemble thus constitutes a powerful tool for addressing our scientific questions. Moreover, it is not important whether each

Table 2
Model Adjustments Used in the 2D Simulation Ensemble

Notation	Description	Intended effect
u0	Domain-averaged horizontal wind is nudged to zero on a one-hour timescale	promote aggregation[a]
SSTa1	Sinusoidal SST distribution (299 K at domain edges and 301 K in the center with a mean of 300 K)	promote aggregation since convection clusters over the warmest SSTs[b]
sfchomo	Interactively computed surface fluxes are horizontally homogenized to the domain average at each time step	inhibit aggregation[c]
radhomo	Interactively computed radiative heating rates are horizontally homogenized to the domain average at each time step	inhibit aggregation[c]
noacre	Cloud radiative effects are turned off.	inhibit aggregation[d]
5xVT	The fall speed of rain is multiplied by a factor of 5 to shorten the residence time of rain in the atmosphere and reduce evaporative cooling	promote aggregation by inhibiting the formation of cold pools[e]
5xACC	The rate of accretion of cloud droplets by rain is multiplied by a factor of 5 to decrease cloud droplet residence time	inhibit stable layer formation due to cloud droplet evaporation[f]
nomelt	Ice cannot melt; it must either sublimate (which can only occur at $T < 273.15$ K) or fall to the surface	inhibit stable layer formation due to melting[g]
RADCAM	Uses the radiation scheme from the Community Atmosphere Model 3[h] rather than RRTM	provide another possible climate realization

[a]Held et al. (1993). [b]Lindzen and Nigam (1987). [c]Bretherton et al. (2005). [d]Pope et al. (2021). [e]Jeevanjee and Romps (2013). [f]Posselt et al. (2008). [g]B. E. Mapes and Houze (1995). [h]Collins et al. (2004).

adjustment actually achieves its intended effect listed in Table 2, so long as the full ensemble encompasses a range of aggregation states.

Apart from the various adjustments, all other aspects of the 2D simulations follow the RCEMIP protocol. The domain is 5,832 km long with 3-km horizontal resolution. For computational reasons, the vertical grid excludes the uppermost two levels of the standard RCEMIP grid. The runs are initialized with an equilibrium sounding from a 3D RCE run with 300-K SSTs and are integrated for 150 days, with full instantaneous output collected every 3 hr. The final 60 days of each run are used to perform the transformation to moisture space described in Section 2.2. In some of the subsequent figures, results are shown for each individual run; in others, we split the 2D ensemble into terciles based on σ^2_{CRH} and compute averages for each tercile. The most and least aggregated terciles contain 7 runs each, while the middle tercile contains 6.

3.2. Circulation and Mean Climate

The various model adjustments used in the 2D runs successfully produce a range of aggregation states (Figures S1 and S2 in Supporting Information S1), and the ensemble captures several known impacts of aggregation on mean climate. These trends are illustrated in Figure 4, in which the color of each line corresponds to the degree of aggregation (red is high σ^2_{CRH}). Aggregation is associated with tropospheric warming (Figure 4a), greater midlevel stability (4b), lower mean RH (4c), and reduced high cloud fraction (4d). The profiles shown in Figure 4 are domain averages; Figures S4–S8 in Supporting Information S1 show the complete distributions of RH, Q_{rad}, static stability, cloud fraction, and D_{rad} in moisture space.

The circulation response to aggregation can be seen in Figure 5, which shows the mean Ψ for each of the σ^2_{CRH} -based terciles (Figure S3 in Supporting Information S1 shows Ψ for each individual run). Nearly all of the simulations produce a trimodal circulation, and the relative strength of the three modes clearly changes with aggregation. As in the RCEMIP ensemble, the congestus cell strengthens with aggregation and even dominates the deep circulation in the most aggregated runs. Congestus invigoration evidently comes at the expense of the shallow circulation, which is also apparent in the profiles of v at the 50th CRH percentile (Figure 4g). In the unaggregated runs, there is strong shallow outflow (negative v) at ∼900 hPa and very weak congestus outflow. In the aggregated runs, the congestus outflow strengthens by a factor of ∼5 and the shallow outflow weakens. This trade-off is unexpected considering the previous finding that shallow circulations promote aggregation (Bretherton et al., 2005; C. J. Muller & Held, 2012). We suspect that the weakening of the shallow circulation is

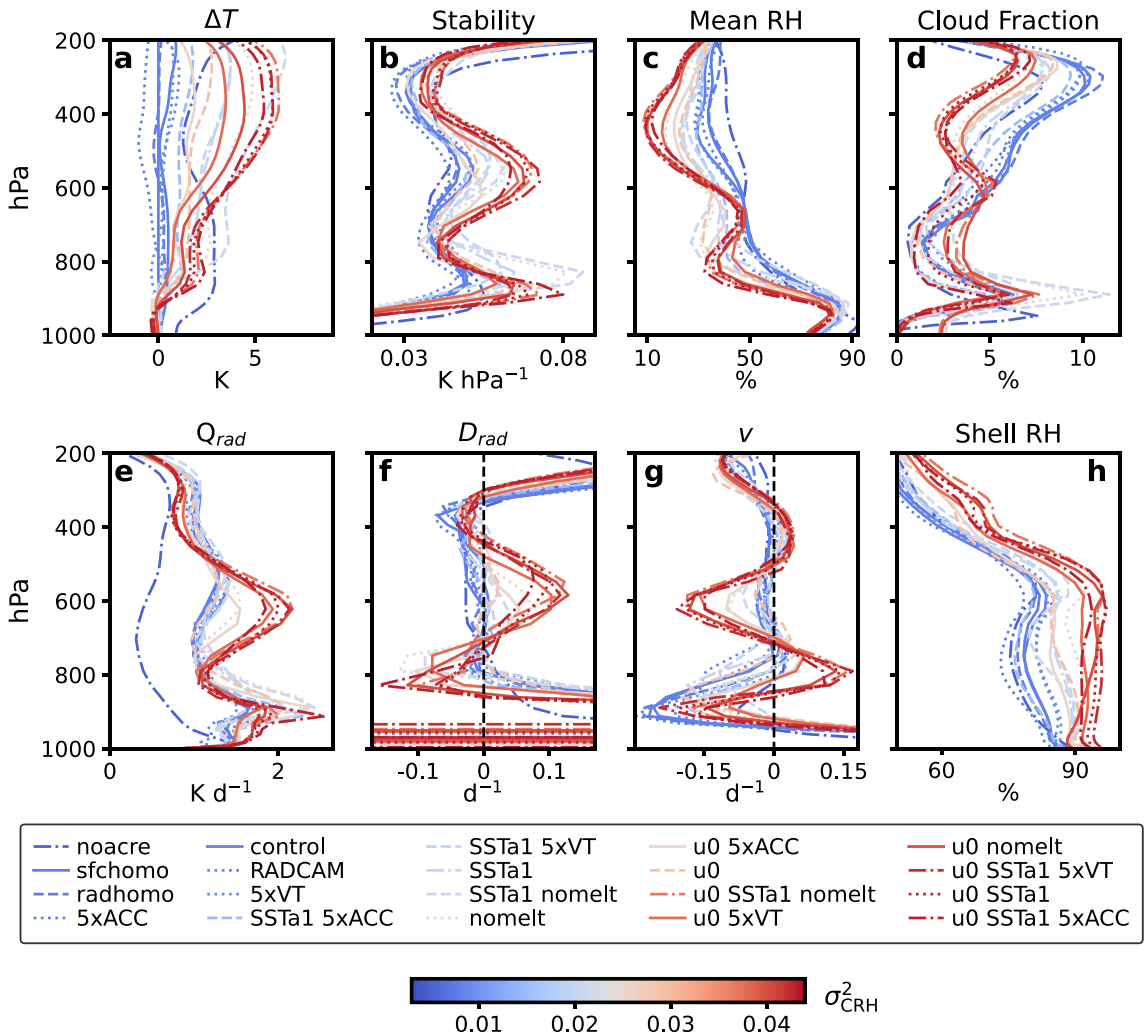

Figure 4. Selected profiles from the 2D runs, with the color of each line corresponding to the degree of aggregation. (a) Temperature anomaly ΔT with respect to the control run, (b) static stability, (c) mean RH, (d) cloud fraction, (e) radiative cooling rate Q_{rad}, (f) radiatively driven divergence D_{rad}, (g) horizontal velocity v at the 50th column relative humidity (CRH) percentile, and (h) RH within 9 km of a convective updraft. With the exception of (g), all profiles are domain averages.

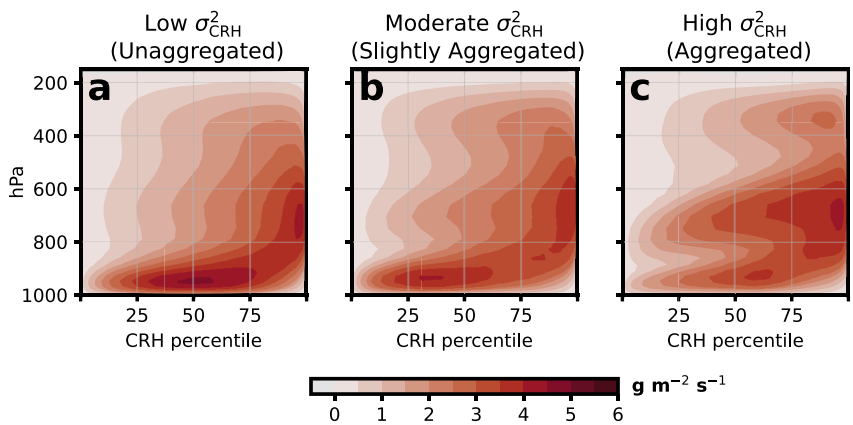

Figure 5. Stream functions for the 2D ensemble, shown as the average of the stream functions from the 6–7 simulations falling within each σ^2_{CRH} tercile. (a) $\sigma^2_{CRH} < 0.011$ (b) $0.011 < \sigma^2_{CRH} < 0.028$ (c) $\sigma^2_{CRH} > 0.028$.

in part due to the formation of a strong inflow (positive v) layer above the boundary layer in the aggregated runs, which may interfere with the shallow convective outflow that would otherwise occur at a similar level. The inflow is seemingly forced by convergence of the radiatively driven subsidence (negative D_{rad}) between 800 and 900 hPa at low CRH percentiles (Figures 4f and S8 in Supporting Information S1). This convergence, which is weak or absent in the unaggregated runs, works against the radiatively driven divergence at the top of the boundary layer that normally draws outflow from the convecting regions. This competition between the shallow and congestus circulations is worthy of closer study but is not our primary focus here.

The 2D ensemble exhibits the various components of the radiative-divergence feedback and allows us to assess why the feedback is amplified by aggregation. Figure 4f shows that the aggregated runs have a peak in radiatively driven divergence at the congestus level, while the unaggregated runs are approximately nondivergent there. This difference arises from a change in the vertical structure of the radiative cooling rate Q_{rad} (Figure 4e). In the unaggregated runs, Q_{rad} is relatively uniform above the boundary layer. As convection aggregates, Q_{rad} nearly doubles in the mid-troposphere and decreases slightly aloft, creating a sharp gradient between 400 and 600 hPa. The shift generally reflects changes in the nonconvective regions, which occupy a majority of the domain (Figures S5 and S8 in Supporting Information S1).

The changes in Q_{rad} and D_{rad} with aggregation are ultimately driven by changes in the distribution of moisture. Aggregation is associated with a reduction in RH throughout the free troposphere, but the 600–700 hPa layer is an important exception. At that level, the aggregated runs are moistened by congestus outflow and have a mean RH similar to the unaggregated runs (Figure 4c). Despite similar RH there, the aggregated runs undergo much stronger radiative cooling because aggregation reduces the emissivity of the upper troposphere. The reduction in emissivity results from upper tropospheric drying and reduced high cloud amount, which simultaneously allow the midlevel moist layer to cool more efficiently and inhibit cooling aloft, since there is less water vapor there to do the emission. The combination of stronger congestus-level cooling and weaker cooling aloft creates the large Q_{rad} gradient that ultimately generates midlevel divergence.

The important insight here is that changes in the distribution of moisture with aggregation allow the radiative-divergence feedback to flourish. The formation of a dry patch with aggregation is crucial because it fosters radiatively driven divergence at the congestus level. Without aggregation, the upper troposphere stays moist, congestus outflow plumes cannot cool as strongly, and there is little or no divergence.

3.3. Mechanisms of Congestus Invigoration

The radiative-divergence mechanism of congestus invigoration is distinct, but not mutually exclusive, from the stability mechanism. To understand the relative importance of the two, we conduct another 2D simulation in which we artificially inflate D_{rad} in the absence of aggregation and its associated increase in stability. To do so, the radiative cooling rate is prescribed as the mean Q_{rad} profile from one of the highly aggregated runs; here we use *u0 5xVT*, but the results are similar if another aggregated run is used. The prescribed radiative cooling is horizontally uniform, which prevents aggregation. The *u0* and *5xVT* adjustments are not actually applied, and everything else about the prescribed radiation (PR) run is identical to the control.

Results from the PR run are shown in Figure 6. The temperature profile in the PR run is free to vary but stays within 1 K of the control run profile up to 300 hPa. As a result, midlevel stability remains close to the control (Figure 6a). On the other hand, the vertical structure of D_{rad} is more similar to the aggregated run, which is by design (Figure 6c). So, the PR run allows the radiative-divergence feedback to operate, albeit artificially, captures the aggregation-related increase in mean D_{rad} without the increase in stability that would normally accompany it.

How does this affect the congestus circulation? In the PR run, v_{cong} changes very little from its value in the control run, which seemingly suggests that the increase in D_{rad} alone does not invigorate the congestus circulation. However, it is important to remember that v_{cong} is simply a measure of the strength of the horizontal flow from high to low CRH. This is different than the amount of congestus-level detrainment from convection, which we quantify as the convergence of the in-cloud mass flux, $-\partial_p \omega_{CLD}$. In the rest of the 2D ensemble, v_{cong} and $-\partial_p \omega_{CLD}$ are tightly coupled (Figure S9 in Supporting Information S1) because strong radiatively driven divergence occurs in low-CRH regions while convection occurs in high-CRH regions; as a result, nearly all of the mass detrained from convection flows toward lower CRH to satisfy mass continuity there. This is not the case in the PR run, in which the prescribed cooling is horizontally uniform and D_{rad} is decoupled from CRH. While some of the mass

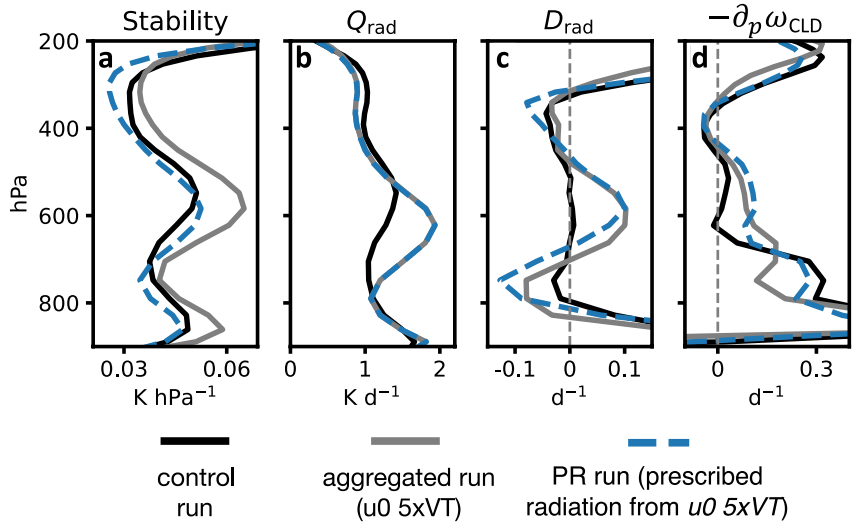

Figure 6. Results from the prescribed radiation (PR) run. (a) Static stability, (b) radiative cooling rate Q_{rad}, (c) radiatively driven divergence D_{rad}, and (d) convergence of the in-cloud mass flux $-\partial_p \omega_{CLD}$. All profiles are domain averages. Clouds are defined as grid boxes with a cloud condensate mixing ratio exceeding 10^{-5} kg/kg.

detrained from convection must still flow toward low CRH to satisfy continuity there, some of it must also remain at high CRH to satisfy the local divergence that we have imposed, resulting in a decrease in the magnitude of v_{cong} relative to $-\partial_p \omega_{CLD}$. Thus, for equal domain-averaged D_{rad}, the PR run will have similar $-\partial_p \omega_{CLD}$ but smaller v_{cong} than a run with interactive radiation. Figure 6d shows that congestus-level $-\partial_p \omega_{CLD}$ in the PR run is similar to the aggregated run, which confirms that congestus-level detrainment scales with the mean D_{rad}. This result is to be expected for an atmosphere in RCE; since convective heating must exactly balance radiative cooling, the prescribed decrease in Q_{rad} with height between 600 and 400 hPa requires the convective heating rate to also decrease with height. This manifests as convective mass flux convergence (i.e., detrainment) at the same level.

The PR run shows that the increase in congestus-level *detrainment* with aggregation can be attributed to the concurrent increase in domain-averaged D_{rad}; the increase in midlevel stability is not necessary. However, invigoration of the congestus *circulation* in moisture space requires horizontal gradients in D_{rad} and does not occur when radiative cooling is horizontally uniform. When radiation is interactive, the formation of a dry patch with aggregation allows for both an increase in domain-averaged D_{rad} and the development of strong D_{rad} gradients. The takeaway here is that the radiative-divergence feedback, rather than the increase in midlevel stability, is responsible for congestus invigoration. This leads us to our final question: what is the nature of the stability response to aggregation? Does it have anything to do with congestus invigoration?

3.4. Summary

- In the 2D RCE ensemble, aggregation invigorates congestus overturning at the expense of the shallow circulation.
- Aggregation creates a favorable environment for the radiative-divergence feedback by reducing the emissivity of the upper troposphere.
- A simulation with prescribed radiation shows that greater radiatively driven divergence leads to more congestus detrainment even when there is no increase in static stability.

4. Why Does Static Stability Increase With Aggregation?

We focus now on the increase in tropospheric static stability that accompanies aggregation and congestus invigoration (Figure 4b). While we have established that the stability increase is not critical for congestus invigoration in the 2D RCE runs, we remain interested in its causes and its relationship to the congestus mode.

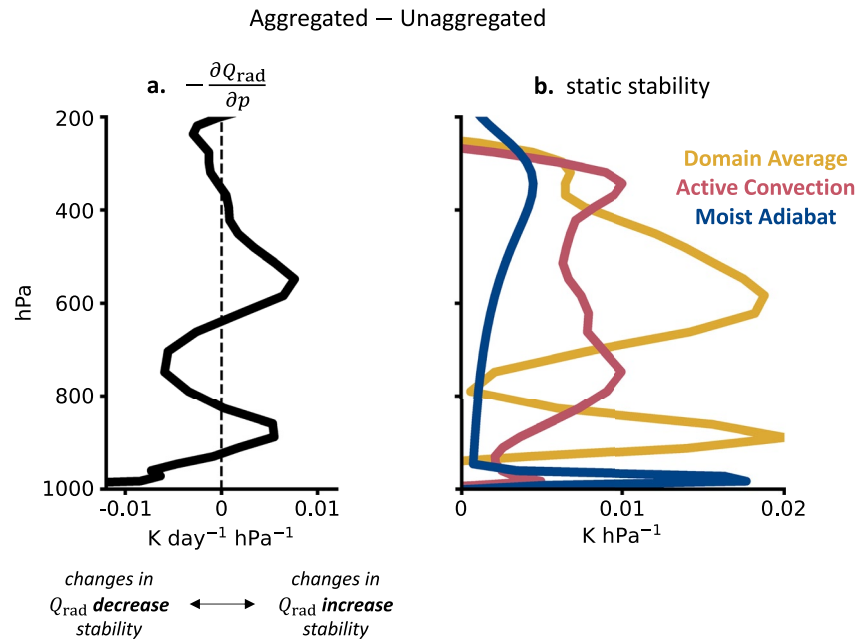

Figure 7. Difference between aggregated and unaggregated 2D runs in (a) the vertical gradient in radiative cooling and (b) three different static stability profiles. Yellow: domain-averaged stability; red: stability in grid boxes containing active convection; blue: stability of an undiluted moist adiabat computed as described in the text.

To simplify our discussion, we compare the mean stability profiles for the most and least aggregated terciles of the 2D ensemble runs. The yellow line in Figure 7b shows the change in domain-averaged stability between the unaggregated and aggregated terciles. Stability increases everywhere between 250 and 950 hPa, with the largest increases at the congestus level and the top of the boundary layer. Our goal here is to determine the causes of the stability increase and to explain its vertical structure.

Previous work has typically attributed the stability increase to changes in convective processes (we will discuss the exact mechanisms shortly). The red line in Figure 7b shows the change in stability within portions of the model domain that are actively convecting, which we define as those with a 400–600-hPa mean ω less than -5 Pa s^{-1} and total condensate mixing ratio greater than 10^{-5} kg kg^{-1}. Within active convection, stability increases with aggregation at all tropospheric levels. But the vertical structure of the stability change looks nothing like that of the change in domain-averaged stability. At the congestus level and at the top of the boundary layer, the increase in domain-averaged stability is much greater than one would expect from the changes within active convection, while the opposite is true in other levels. This tells us that the mean RCE temperature profile is not simply "set" by deep convection. While changes in convective processes provide a baseline increase in stability throughout the troposphere, radiative processes are also important, and the effect of these processes on the mean temperature profile evidently changes with aggregation. In the remainder of this section, we discuss and evaluate the convective and radiative sources of enhanced stability.

4.1. Convective Sources

Why does the static stability within active convection increase with aggregation? Here, we discuss two explanations from the literature and evaluate their importance in the 2D ensemble.

The first explanation is that aggregation increases the initial moisture content of convective updrafts, which causes convection to follow a warmer, more stable moist adiabat. Held et al. (1993) suggested that the increase in initial moisture content occurs because convection begins closer to the surface, where it is more humid. But in the 2D ensemble, aggregation is associated with a *decrease* in the fraction of actively convecting columns that have upward motion throughout the boundary layer, so this mechanism does not explain the present results. Alternatively, Bretherton et al. (2005) found that the near-surface RH in convective regions increases with aggregation, which would boost the initial moisture content of updrafts without any change in their initiation height. In the

2D ensemble, aggregation is indeed associated with an increase in boundary layer RH in convective regions. We assess the impact of this increase on stability by computing moist adiabatic temperature profiles (and associated stability profiles) for each run, using as the starting point the 1000-hPa temperature and RH in the top CRH percentile, where most of the upward convective mass flux occurs. The moist adiabats are computed using the MetPy Python package, which computes saturated pseudoadiabats neglecting the difference in saturation vapor pressure over liquid and ice (May et al., 2008). The blue line in Figure 7b shows the change in moist adiabatic stability between the aggregated and unaggregated terciles. The magnitude of the increase is far too small to account for the increase in stability within active convection, so we can conclude that changes in surface RH play only a minor role in the stability response to aggregation. This result is not sensitive to the exact level at which the moist adiabats are initialized.

The second explanation deals not with the initial moisture content of convection but with the impact of entrainment mixing once convection has begun. The tropical temperature profile deviates from a perfect moist adiabat due to the entrainment of unsaturated air into convective updrafts, which leads to evaporation and causes the lapse rate to exceed that of an undiluted plume (Singh & O'Gorman, 2013). It has been hypothesized that aggregation mitigates this entrainment cooling (B. Mapes & Neale, 2011; Feng et al., 2015), leading to an increase in stability. Large-eddy and convection-permitting simulations support this prediction, but with an important caveat: the reduction in entrainment cooling does not occur because entrainment itself is reduced (in fact, the opposite occurs) but rather because the entrained environmental air is more humid and thus cannot cause as much evaporative cooling (Becker et al., 2018; Becker & Hohenegger, 2021). In essence, aggregation creates a "moist shell" that protects convective plumes from entrainment cooling (Becker et al., 2018). This is physically intuitive, considering that what it means to be aggregated in the first place is that convection occurs in the vicinity of other convection, where it is already likely to be moist. But aggregation as indicated by large σ^2_{CRH} by no means guarantees the presence of a moist shell. First of all, CRH is skewed toward the RH of the warm lower troposphere and therefore provides limited information about RH at higher levels. Furthermore, as shown by Figure 1 and S1 in Supporting Information S1, variability in σ^2_{CRH} is driven mostly by how dry the dry regions are, which tells us nothing about the RH distribution in moist regions.

Is a moist shell detectable in our 2D simulations? We define the convective shell as the portion of the model domain that is within three grid boxes (9 km) of active convection but is not actively convecting itself. Figure 4h shows that the mean shell RH increases with aggregation throughout the entire troposphere. It is not surprising to see this result at the level of congestus detrainment, since congestus invigoration itself moistens the convective shell there. But the greatest difference in shell RH (10%–15%) is found below this level, between 700 and 900 hPa. Relative to an unaggregated shell RH of 80%, a 10%–15% increase constitutes a 50%–75% reduction in saturation deficit, suggesting that the moist shell effect has a substantial impact on the efficiency of entrainment cooling. Within the 700–900 hPa layer, the within-convection stability becomes increasingly sensitive to aggregation with height (Figure 7b), which is consistent with the accumulating impact of the moist shell on a rising parcel. Of course, some of the impact may be offset if the entrainment rate increases with aggregation, as was found by Becker et al. (2018). While an in-depth study of entrainment rates is beyond our scope here, the development of a moist shell with aggregation and the insufficiency of the alternative explanations both suggest that the moist shell plays an important role in stability enhancement. These results are not sensitive to the threshold used to define the convective shell.

4.2. Radiative Sources

We have now shown that decreases in entrainment cooling are likely more important than increases in surface RH when it comes to the increase in stability within active convection. We now turn to radiative sources of increased stability.

Posselt et al. (2008) suggested that differential radiative cooling at the top of congestus outflow layers could lead to enhanced stability, as the moist outflow layer cools more rapidly than the dry air immediately above. As we have already shown, the vertical gradient of Q_{rad} in the mid-troposphere is stronger when convection is aggregated. This is illustrated again in Figure 7a, which shows the difference in $-\partial_p Q_{\mathrm{rad}}$ (where $\partial_p = \partial/\partial p$) between the aggregated and unaggregated terciles. At levels where $-\partial_p Q_{\mathrm{rad}}$ increases with aggregation (350–650 and 825–900 hPa), changes in the Q_{rad} profile are acting to increase stability. Comparison of Figures 7a and 7b shows that this occurs where the increase in domain-averaged stability exceeds that within active convection.

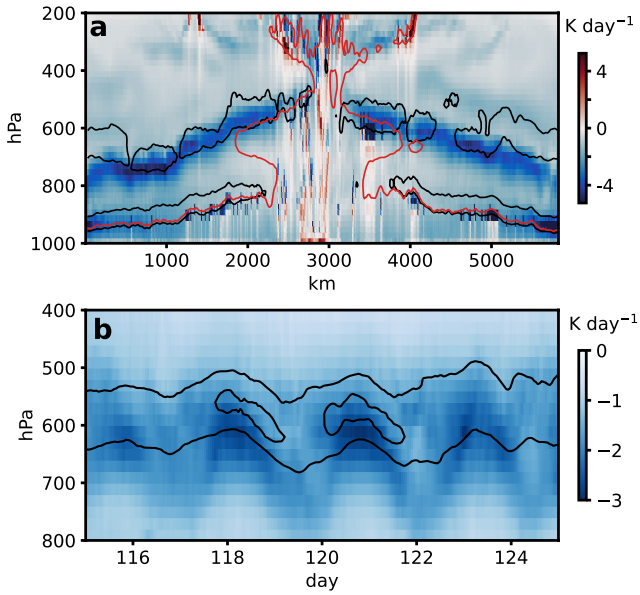

Figure 8. Stability and radiative cooling in one of the highly aggregated 2D runs (*u0 SSTa1 5xVT*). (a) Colored shading shows the instantaneous radiative heating rate. The black contour indicates static stability in excess of 0.075 K hPa^{-1} and the red contour shows relative humidity above 60%. (b) Blue shading shows the domain-averaged radiative heating rate over a 10-day period. Black contours indicate domain-averaged stability of 0.065 and 0.073 K day^{-1}.

The opposite is true where changes in $-\partial_p Q_{\text{rad}}$ act to decrease stability. The structural similarity between the changes in differential radiative cooling and the changes in domain-averaged stability suggest that the former plays an important role in shaping the latter.

How can we be sure that the link between differential radiative cooling and enhanced mean stability is causal? Examining their association over space and time provides compelling evidence. Figure 8a shows an instantaneous snapshot of stability and Q_{rad} in one of the highly aggregated runs (*u0 SSTa1 5xVT*). The convective region is in the center of the domain, where the SST is slightly elevated. The sloping bands of strong radiative cooling mark the top of the congestus outflow layer. Stable layers, enclosed by the black contours, are found at the top of the outflow layer and remain linked to it as it subsides. In the driest regions (both ends of the periodic domain), the stable layer has detached from the outflow layer and is located just above it. We speculate that this has to do with the horizontal spreading of stability anomalies by gravity waves emanating out from convection. After detrainment, stability anomalies grow via differential cooling at the top of the outflow layer as it subsides. Eventually, the stability anomalies are "ripped off" of the outflow layer by gravity waves, which work to erase the horizontal temperature gradients that develop from the vertical displacement of the stability anomaly.

The link between stability and differential radiative cooling can also be seen over time. Figure 8b shows the domain-averaged stability and Q_{rad} over a 10-day period in the same aggregated run. Bands of strong radiative cooling originate at the congestus outflow level approximately every 2.5 days. These oscillations have been noted in previous work and have a period that depends on the size of the model domain (Grabowski et al., 2000). Stability anomalies can be seen growing at the top of the outflow plumes and subsiding with them. At a fixed pressure level, stability is greatest when there is strong differential radiative cooling.

4.3. Summary

- The static stability response to aggregation in the 2D ensemble is shaped by both convective and radiative processes; both are of similar importance.
- In convective regions, a reduction in entrainment cooling with aggregation is a more plausible driver of increased stability than changes in surface RH. These changes are not directly related to congestus invigoration.
- In nonconvective regions, strong differential Q_{rad} at the top of congestus outflow plumes act to increase midlevel stability. This change is directly tied to congestus invigoration.

5. Discussion

This paper began with a discussion of the third mode of tropical convection: the congestus mode. We examined congestus representation and variability in the RCEMIP CRM ensemble and in a new ensemble of 2D RCE simulations conducted with SAM, a widely used cloud-resolving model. A wide variety of congestus representations were found in both ensembles, underscoring the need to better understand the nature of the congestus mode in cloud-resolving RCE.

The most significant finding of this work is that the congestus mode is invigorated by large-scale convective aggregation. The invigoration mechanism is, at its core, very similar to that which is thought to drive shallow circulations at the top of the boundary layer. Both rely on the presence of sharp vertical gradients in the longwave cooling rate, which are ultimately caused by sharp gradients in moisture. In the shallow circulation case, these gradients are found at the top of the moist boundary layer, whereas in the congestus case they are found at the top of congestus outflow plumes. Aggregation is an important part of this process because it dries out the upper troposphere in nonconvecting regions, which allows for stronger cooling at the top of the moist layer. This invigoration mechanism relies on basic principles of radiative transfer and mass conservation, and its components are

present in both the RCEMIP and 2D RCE ensembles. While the impact of aggregation on congestus overturning is clear, whether or not the congestus mode affects initiation and development of aggregation remains uncertain.

Notably, congestus invigoration in the 2D ensemble is accompanied by a slowdown of the shallow circulation. This may be explained by radiatively driven convergence just above the dry-region boundary layer, which drives dry-to-moist convective inflow at the level where shallow convective outflow would otherwise be found. Further study of this apparent competition between the shallow and congestus modes would be worthwhile and would improve our understanding of convective dynamics.

This work also examined how static stability affects and is affected by congestus invigoration. Previous work has largely assumed that mid-tropospheric stable layers are the cause of congestus-level detrainment. With this logic, congestus invigoration might be attributed to an increase in midlevel stability. But the results presented in Sections 3.3 and 4 suggest that enhanced stability is largely the result, rather than the cause, of congestus invigoration. The crux of this finding was a model experiment showing that congestus-level detrainment increases without any change in stability in response to a prescribed increase in the mean radiatively driven divergence. It is important to reiterate that this result may be inevitable in simple RCE simulations such as these, in which any imposed gradient in radiative cooling must be matched by a gradient in convective heating. For this reason, we caution that this specific result may be limited in scope, and it is unclear to what extent it applies to the real tropics, where approximate RCE is realized only on large spatial timescales (Jakob et al., 2019).

In Section 4, we asked why the mean static stability increases as convection aggregates. Much of this stability enhancement can be attributed to congestus invigoration: stability anomalies grow by differential radiative cooling atop congestus outflow plumes before being smoothed out by gravity waves. The stability increase is likely supported by a moistened convective shell, which reduces the efficiency of entrainment cooling and allows convecting parcels to adhere more closely to a moist adiabatic temperature profile. Aggregation also increases the surface RH in convecting regions, but this has a relatively small impact on stability compared to the other factors. These results are helpful for understanding the sensitivity of mean climate to aggregation, and they illustrate how the response to aggregation can be significantly affected by congestus dynamics. Our understanding of the stability response to aggregation would benefit from simulations with finer horizontal resolution, which would provide a more complete picture of entrainment processes.

This work leaves us with many questions worthy of further study. How is congestus overturning affected by climate warming? The answer to this question will almost certainly depend on how warming affects the degree of convective aggregation, which remains very uncertain. And how may the congestus circulation itself affect the climate sensitivity of the RCE state? Given its impacts on moisture and radiative transfer, we suspect that congestus strength has a direct bearing on the surface and top-of-atmosphere energy budgets. Perhaps most importantly, how realistic are model representations of the congestus mode? Without a doubt, the findings reported here are helpful for understanding RCE simulated by cloud-resolving models. Their applicability to the real world remains an open question.

Deepening our knowledge of how clouds, convection, and circulation interact is a pressing priority within climate science and is critical to the advancement of the field (Bony et al., 2016). Cloud-resolving RCE simulations, such as those discussed here, have proven to be a valuable research tool in this endeavor. As we have shown, RCE climates can be greatly affected by the congestus mode. Careful interpretation of cloud-resolving RCE therefore requires continued study of the "forgotten mode" of tropical convection.

Data Availability Statement

We also thank the group of scientists who provided simulations for RCEMIP and the German Climate Computing Center (DKRZ) for hosting the standardized RCEMIP data, which is publicly available at http://hdl.handle.net/21.14101/d4beee8e-6996-453e-bbd1-ff53b6874c0e. Composited model output for the 2D SAM ensemble is available at http://hdl.handle.net/1773/48345.

Acknowledgments
This work was supported by NASA FINESST Grant 80NSSC20K1613 and NSF grant AGS-2124496. We thank Martin Singh and Benjamin Fildier for their thoughtful comments and suggestions and Peter Blossey for his insights and assistance with the SAM model code.

References

Arnold, N. P., & Putman, W. M. (2018). Nonrotating convective self-aggregation in a limited area AGCM. *Journal of Advances in Modeling Earth Systems*, *10*(4), 1029–1046. https://doi.org/10.1002/2017MS001218

Becker, T., Bretherton, C. S., Hohenegger, C., & Stevens, B. (2018). Estimating bulk entrainment with unaggregated and aggregated convection. *Geophysical Research Letters*, *45*(1), 455–462. https://doi.org/10.1002/2017GL076640

Becker, T., & Hohenegger, C. (2021). Entrainment and its dependency on environmental conditions and convective organization in convection-permitting simulations. *Monthly Weather Review*, *149*(2), 537–550. https://doi.org/10.1175/MWR-D-20-0229.1

Beydoun, H., & Hoose, C. (2019). Aerosol-cloud-precipitation interactions in the context of convective self-aggregation. *Journal of Advances in Modeling Earth Systems*, *11*(4), 1066–1087. https://doi.org/10.1029/2018MS001523

Bony, S., Stevens, B., Coppin, D., Becker, T., Reed, K. A., Voigt, A., & Medeiros, B. (2016). Thermodynamic control of anvil cloud amount. *Proceedings of the National Academy of Sciences*, *113*(32), 8927–8932. https://doi.org/10.1073/pnas.1601472113

Bretherton, C. S., Blossey, P. N., & Khairoutdinov, M. (2005). An energy-balance analysis of deep convective self-aggregation above uniform SST. *Journal of the Atmospheric Sciences*, *62*(12), 4273–4292. https://doi.org/10.1175/JAS3614.1

Bretherton, C. S., Blossey, P. N., & Peters, M. E. (2006). Interpretation of simple and cloud-resolving simulations of moist convection–radiation interaction with a mock-Walker circulation. *Theoretical and Computational Fluid Dynamics*, *20*(5), 421–442. https://doi.org/10.1007/s00162-006-0029-7

Chen, Y.-C., & Yu, J.-Y. (2021). Modes of tropical convection and their roles in transporting moisture and moist static energy: Contrast between deep and shallow convection. *Climate Dynamics*, *57*(7–8), 1789–1803. https://doi.org/10.1007/s00382-021-05777-x

Chen, Y.-T., & Wu, C.-M. (2019). The role of interactive SST in the cloud-resolving simulations of aggregated convection. *Journal of Advances in Modeling Earth Systems*, *11*(10), 3321–3340. https://doi.org/10.1029/2019MS001762

Collins, W. D., Rasch, P. J., Boville, B. A., Hack, J. J., McCaa, J. R., Williamson, D. L., et al. (2004). *Description of the NCAR community atmosphere model (CAM 3.0)*. (Tech. Rep. Nos. NCAR Tech. Note NCAR/TN-464+STR.

Feng, Z., Hagos, S., Rowe, A. K., Burleyson, C. D., Martini, M. N., & de Szoeke, S. P. (2015). Mechanisms of convective cloud organization by cold pools over tropical warm ocean during the AMIE/DYNAMO field campaign. *Journal of Advances in Modeling Earth Systems*, *7*(2), 357–381. https://doi.org/10.1002/2014MS000384

Grabowski, W. W., Yano, J.-I., & Moncrieff, M. W. (2000). Cloud resolving modeling of tropical circulations driven by large-scale SST gradients. *Journal of the Atmospheric Sciences*, *57*(13), 2022–2040. https://doi.org/10.1175/1520-0469(2000)057

Held, I. M., Hemler, R. S., & Ramaswamy, V. (1993). Radiative-convective equilibrium with explicit two-dimensional moist convection. *Journal of the Atmospheric Sciences*, *50*(23), 3909–3927. (Publisher: American Meteorological Society Section: Journal of the Atmospheric Sciences). https://doi.org/10.1175/1520-0469(1993)050

Holloway, C. E., & Woolnough, S. J. (2016). The sensitivity of convective aggregation to diabatic processes in idealized radiative-convective equilibrium simulations. *Journal of Advances in Modeling Earth Systems*, *8*(1), 166–195. https://doi.org/10.1002/2015MS000511

Iacono, M. J., Mlawer, E. J., Clough, S. A., & Morcrette, J.-J. (2000). Impact of an improved longwave radiation model, RRTM, on the energy budget and thermodynamic properties of the NCAR community climate model, CCM3. *Journal of Geophysical Research*, *105*(D11), 14873–14890. https://doi.org/10.1029/2000JD900091

Jakob, C., Singh, M. S., & Jungandreas, L. (2019). Radiative convective equilibrium and organized convection: An observational perspective. *Journal of Geophysical Research: Atmospheres*, *124*(10), 5418–5430. https://doi.org/10.1029/2018JD030092

Jeevanjee, N., & Romps, D. M. (2013). Convective self-aggregation, cold pools, and domain size. *Geophysical Research Letters*, *40*(5), 994–998. https://doi.org/10.1002/grl.50204

Johnson, R. H., Ciesielski, P. E., & Hart, K. A. (1996). Tropical inversions near the 0°C level. *Journal of the Atmospheric Sciences*, *53*(13), 1838–1855. https://doi.org/10.1175/1520-0469(1996)053

Johnson, R. H., Rickenbach, T. M., Rutledge, S. A., Ciesielski, P. E., & Schubert, W. H. (1999). Trimodal characteristics of tropical convection. *Journal of Climate*, *12*(8), 2397–2418. https://doi.org/10.1175/1520-0442(1999)012

Khairoutdinov, M. F., & Randall, D. A. (2003). Cloud resolving modeling of the ARM summer 1997 IOP: Model formulation, results, uncertainties, and sensitivities. *Journal of the Atmospheric Sciences*, *60*(4), 607–625. https://doi.org/10.1175/1520-0469(2003)060

Lindzen, R. S., & Nigam, S. (1987). On the role of sea surface temperature gradients in forcing low-level winds and convergence in the tropics. *Journal of the Atmospheric Sciences*, *44*(17), 2418–2436. https://doi.org/10.1175/1520-0469(1987)044

Mapes, B., & Neale, R. (2011). Parameterizing convective organization to escape the entrainment dilemma. *Journal of Advances in Modeling Earth Systems*, *3*(2). https://doi.org/10.1029/2011MS000042

Mapes, B. E., & Houze, R. A. (1995). Diabatic divergence profiles in western Pacific mesoscale convective systems. *Journal of the Atmospheric Sciences*, *52*(10), 1807–1828. https://doi.org/10.1175/1520-0469(1995)052

Mapes, B. E., & Zuidema, P. (1996). Radiative-dynamical consequences of dry tongues in the tropical troposphere. *Journal of the Atmospheric Sciences*, *53*(4), 620–638. https://doi.org/10.1175/1520-0469(1996)053

Masunaga, H., & L'Ecuyer, T. S. (2014). A mechanism of tropical convection inferred from observed variability in the moist static energy budget. *Journal of the Atmospheric Sciences*, *71*(10), 3747–3766. (Publisher: American Meteorological Society Section). https://doi.org/10.1175/JAS-D-14-0015.1

May, R., Arms, S., March, P., Bruning, E., & Leeman, J. (2008). *MetPy: A Python package for meteorological data*. https://doi.org/10.5065/D6WW7G29

Mlawer, E. J., Taubman, S. J., Brown, P. D., Iacono, M. J., & Clough, S. A. (1997). Radiative transfer for inhomogeneous atmospheres: RRTM, a validated correlated-k model for the longwave. *Journal of Geophysical Research*, *102*(D14), 16663–16682. https://doi.org/10.1029/97JD00237

Morrison, H., & Milbrandt, J. A. (2015). Parameterization of cloud microphysics based on the prediction of bulk ice Particle properties. Part I: Scheme description and idealized tests. *Journal of the Atmospheric Sciences*, *72*(1), 287–311. https://doi.org/10.1175/JAS-D-14-0065.1

Muller, C., & Bony, S. (2015). What favors convective aggregation and why? *Geophysical Research Letters*, *42*(13), 5626–5634. https://doi.org/10.1002/2015GL064260

Muller, C. J., & Held, I. M. (2012). Detailed investigation of the self-aggregation of convection in cloud-resolving simulations. *Journal of the Atmospheric Sciences*, *69*(8), 2551–2565. https://doi.org/10.1175/JAS-D-11-0257.1

Naumann, A. K., Stevens, B., & Hohenegger, C. (2019). A moist conceptual model for the boundary layer structure and radiatively driven shallow circulations in the trades. *Journal of the Atmospheric Sciences*, *76*(5), 1289–1306. https://doi.org/10.1175/JAS-D-18-0226.1

Naumann, A. K., Stevens, B., Hohenegger, C., & Mellado, J. P. (2017). A conceptual model of a shallow circulation induced by prescribed low-level radiative cooling. *Journal of the Atmospheric Sciences*, *74*(10), 3129–3144. https://doi.org/10.1175/JAS-D-17-0030.1

Nigam, S. (1997). The annual warm to cold phase transition in the eastern equatorial Pacific: Diagnosis of the role of stratus cloud-top cooling. *Journal of Climate*, *10*(10), 2447–2467. https://doi.org/10.1175/1520-0442(1997)010

Nishant, N., Sherwood, S. C., & Geoffroy, O. (2016). Radiative driving of shallow return flows from the ITCZ. *Journal of Advances in Modeling Earth Systems*, *8*(2), 831–842. https://doi.org/10.1002/2015MS000606

Nolan, D. S., Zhang, C., & Chen, S. H. (2007). Dynamics of the shallow meridional circulation around intertropical convergence zones. *Journal of the Atmospheric Sciences*, *64*(7), 2262–2285. https://doi.org/10.1175/JAS3964.1

Nuijens, L., & Emanuel, K. (2018). Congestus modes in circulating equilibria of the tropical atmosphere in a two-column model. *Quarterly Journal of the Royal Meteorological Society*, *144*(717), 2676–2692. https://doi.org/10.1002/qj.3385

Pope, K. N., Holloway, C. E., Jones, T. R., & Stein, T. H. M. (2021). Cloud-radiation interactions and their contributions to convective self-aggregation. *Journal of Advances in Modeling Earth Systems*, *13*(9), e2021MS002535. https://doi.org/10.1029/2021MS002535

Posselt, D. J., Heever, S. C. v. d., & Stephens, G. L. (2008). Trimodal cloudiness and tropical stable layers in simulations of radiative convective equilibrium. *Geophysical Research Letters*, *35*(8), L08802. https://doi.org/10.1029/2007GL033029

Schulz, H., & Stevens, B. (2018). Observing the tropical atmosphere in moisture space. *Journal of the Atmospheric Sciences*, *75*(10), 3313–3330. https://doi.org/10.1175/JAS-D-17-0375.1

Singh, M. S., & O'Gorman, P. A. (2013). Influence of entrainment on the thermal stratification in simulations of radiative-convective equilibrium. *Geophysical Research Letters*, *40*(16), 4398–4403. https://doi.org/10.1002/grl.50796

Sobel, A. H., Nilsson, J., & Polvani, L. M. (2001). The weak temperature gradient approximation and balanced tropical moisture waves. *Journal of the Atmospheric Sciences*, *58*(23), 3650–3665. https://doi.org/10.1175/1520-0469(2001)058

Trenberth, K. E., Stepaniak, D. P., & Caron, J. M. (2000). The global monsoon as seen through the divergent atmospheric circulation. *Journal of Climate*, *13*(22), 3969–3993. https://doi.org/10.1175/1520-0442(2000)013

Wing, A. A., & Cronin, T. W. (2016). Self-aggregation of convection in long channel geometry. *Quarterly Journal of the Royal Meteorological Society*, *142*(694), 1–15. https://doi.org/10.1002/qj.2628

Wing, A. A., Reed, K. A., Satoh, M., Stevens, B., Bony, S., & Ohno, T. (2018). Radiative–convective equilibrium model intercomparison project. *Geoscientific Model Development*, *11*(2), 793–813. https://doi.org/10.5194/gmd-11-793-2018

Wing, A. A., Stauffer, C. L., Becker, T., Reed, K. A., Ahn, M., Arnold, N. P., et al. (2020). Clouds and convective self-aggregation in a multi-model ensemble of radiative-convective equilibrium simulations. *Journal of Advances in Modeling Earth Systems*, *12*(9). https://doi.org/10.1029/2020MS002138

Wu, Z. (2003). A shallow CISK, deep equilibrium mechanism for the interaction between large-scale convection and large-scale circulations in the tropics. *Journal of the Atmospheric Sciences*, *60*(2), 377–392. https://doi.org/10.1175/1520-0469(2003)060

Yano, J.-I., Moncrieff, M. W., & Grabowski, W. W. (2002). Walker-type mean circulations and convectively coupled tropical waves as an interacting System. *Journal of the Atmospheric Sciences*, *59*(9), 1566–1577. https://doi.org/10.1175/1520-0469(2002)059

Yasunaga, K., Yoneyama, K., Kubota, H., Okamoto, H., Shimizu, A., Kumagai, H., et al. (2006). Melting layer cloud observed during R/V mirai cruise MR01-K05. *Journal of the Atmospheric Sciences*, *63*(11), 3020–3032. https://doi.org/10.1175/JAS3779.1

Zhang, C., McGauley, M., & Bond, N. A. (2004). Shallow meridional circulation in the tropical eastern Pacific. *Journal of Climate*, *17*(1), 133–139. https://doi.org/10.1175/1520-0442(2004)017

Zhang, C., Nolan, D. S., Thorncroft, C. D., & Nguyen, H. (2008). Shallow meridional circulations in the tropical atmosphere. *Journal of Climate*, *21*(14), 3453–3470. https://doi.org/10.1175/2007JCLI1870.1

Zuidema, P., Mapes, B., Lin, J., Fairall, C., & Wick, G. (2006). The interaction of clouds and dry air in the eastern tropical Pacific. *Journal of Climate*, *19*(18), 4531–4544. https://doi.org/10.1175/JCLI3836.1